Photonic Topological Mode Bound to a Vortex

Adrian J. Menssen,[1,*] Jun Guan,[2,†] David Felce,[1] Martin J. Booth,[2] and Ian A. Walmsley[1,3]
[1]Department of Atomic and Laser Physics, University of Oxford, Oxford OX13PU, United Kingdom
[2]Department of Engineering Science, University of Oxford, Oxford OX13PJ, United Kingdom
[3]Department of Physics Imperial College, London SW72AZ, United Kingdom

(Received 21 January 2020; accepted 17 June 2020; published 10 September 2020)

We report the observation of a mode associated with a topological defect in the bulk of a 2D photonic material by introducing a vortex distortion to a hexagonal lattice analogous to graphene. The observed modes lie midgap at zero energy and are closely related to Majorana bound states in superconducting vortices. This is the first experimental demonstration of the Jackiw-Rossi model [R. Jackiw and P. Rossi, Nucl. Phys. **B190**, 681 (1981)].

DOI: 10.1103/PhysRevLett.125.117401

Introduction.—Phenomena associated with the topological characteristics of physical systems are of wide-reaching interest in many fields in physics, with applications ranging from condensed matter physics [1–3] to particle physics [4,5] and cosmology [6]. Most prominently topology has been applied in condensed matter physics, where the importance of the topology of the band structure was first recognized in the discovery of the integer quantum Hall effect [7]. Subsequently many classes of topological insulators and superconductors have been discovered [2]. A key characteristic of a system with nontrivial topology is the presence of topological invariants, integer numbers that classify the topological structure. They are preserved under smooth, homotopic deformations of the Hamiltonian. At the boundary between domains governed by different such invariants, where the topology abruptly changes, a topological defect occurs. Localized at these defects are states protected by the topology of the system: they are robust to errors in the underlying Hamiltonian. These edge states have been investigated extensively in photonic platforms [8–12]. Their study generated important insight into the physics of topological insulators [10] and spawned technological advances such as the development of topological lasers [13], where lasing occurs in edge states, protected from imperfections. Here, in contrast, we investigate for the first time a state bound to a vortex, a point defect, in the bulk of a 2D photonic material (photonic graphene). These modes are zero modes, as they lie midgap, at zero energy. The vortex-bound zero modes we consider here are of significant interest to solid-state physics. In topological superconductors they support Majorana bound states at the vortex core [2,14–16]. The vortex defects we realize here are photonic analogues of the vortices in topological superconductors explored by Reed, Green [16], and Volovik [15]. Majorana bound states at these vortices are a promising candidate for the realization of a topological quantum computer [17]. The Jackiw-Rossi [5] model was originally introduced in a quantum field theory context to describe fermions in a $2+1$D system coupled to a complex scalar field in the Dirac equation. Jackiw and Rossi [5] demonstrated that if the scalar field contains a vortex it supports localized zero-energy solutions at the vortex core. Witten [6] also considered the Jackiw-Rossi–type vortex defect in the context of superconducting cosmic strings.

Particles in a tight-binding model of graphene can be shown to obey a Dirac equation near the Dirac cones in the band structure. Hou, Chamon, and Mudry [18] predicted zero modes in graphene which realize the Jackiw-Rossi model: Small perturbations to the graphene lattice induce the scalar-field coupling to the effective Dirac equation governing the graphene tight-binding model. A photonic platform allows for a high degree of control over the system parameters and is thus a powerful tool to investigate topological effects, where in solid state systems this degree of control is notoriously difficult to engineer. The vortex topological defect is realized by introducing a distortion to the waveguide position in a hexagonal waveguide lattice as was suggested by Iadecola *et al.* [19]. We show adiabatic transport of the zero mode as the vortex is moved, as well as topological protection against imperfections of the waveguide lattice.

Theory.—The wave function evolution generated by a tight-binding Hamiltonian can be mapped directly to the coupled mode equations of light propagating through a photonic crystal, where the time dimension in the Schrödinger equation takes the role of the propagation direction of the light through the crystal:

$$i\frac{\partial\psi_{\mathbf{r}}(z)}{\partial z}=\sum_{j=1}^{3}H_{\mathbf{r},\mathbf{r}+\mathbf{s_j}}\psi_{\mathbf{r}\pm\mathbf{s_j}}(z), \tag{1}$$

$\psi_{\mathbf{r}}(z)$ is the electric field amplitude at lattice site $\mathbf{r}$ and z is the length of the crystal the light has propagated through, $\mathbf{s_j}$

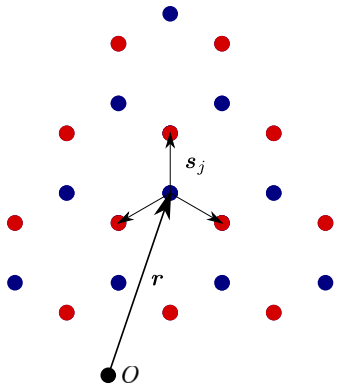

FIG. 1. Hexagonal lattice with two triangular sublattices (A and B) in blue and red, lattice vector $\mathbf{r}$ and vectors between nearest neighbors $\mathbf{s_j}$ indicated.

points to its jth nearest neighbor (see Fig. 1). The complex scalar field $\Delta(\mathbf{r})$ containing the vortex can be simulated by introducing a distortion $\delta_{\mathbf{r},\mathbf{s_j}}$ to the nearest neighbor hopping strength t of graphene [18]:

$$H_{\mathbf{r},\mathbf{r}+\mathbf{s_j}} = -t - \delta_{\mathbf{r},\mathbf{s_j}}$$
$$\delta_{\mathbf{r},\mathbf{s_j}} = \frac{1}{2}\Delta(\mathbf{r})e^{i\mathbf{K}_+\mathbf{s_j}}e^{i2\mathbf{i}\mathbf{K}_+\mathbf{r}} + \text{c.c.}, \tag{2}$$

$\mathbf{K}_+ = [4\pi/(3\sqrt{3}a), 0]$ marks the position of Dirac point in the reciprocal lattice. a is the lattice constant. The explicit form of $\Delta(\mathbf{r})$ containing a vortex at $\mathbf{r} = 0$ is

$$\Delta(\mathbf{r}) = \Delta_0(r)e^{i(\alpha+N\phi)}$$
$$\Delta_0(r) = \Delta_0 \tanh(r/l_0), \tag{3}$$

where ϕ is the polar angle of $\mathbf{r}$, l_0 the width of the vortex, α the phase of the vortex and N the vorticity, the topological invariant of the system. The sign of the vorticity determines which of the two triangular sublattices of graphene (see Fig. 1) supports the mode (1 for sublattice A, -1 for sublattice B). In this work we set its value to 1: the mode is confined to sublattice A, whereas the distortion is applied to sublattice B. For the vortex phase we chose $\alpha = \pi/2$. The radial dependence of the zero mode wave function $\phi_A(r)$ localized on sublattice A [a solution to the mode-coupling equations, Eqs. (1)] is given by [15,18,20]

$$\phi_A(r) \sim e^{i[-(\alpha/2)+(\pi/4)]}e^{-\int_0^r dr'\Delta_0(r')}. \tag{4}$$

The electrical field strength is given by

$$E(\mathbf{r}, z, t) \sim \text{Re}[(\phi_A(r)e^{i\mathbf{K}_+\mathbf{r}} + \text{c.c.})e^{ik_\omega z - i\omega t}], \tag{5}$$

where $\mathbf{r}$ points to a lattice site on the supporting sublattice A. The vortex in $\Delta(\mathbf{r})$ and the zero-mode state bound to it are visualized in Fig. 2(a). The distortions $\delta_{\mathbf{r},\mathbf{s_j}}$ of the coupling Hamiltonian are implemented with small shifts in the waveguides' positions [illustrated in Fig. 2(b)], assuming exponential decay of the field away from the waveguides. The exponential decay was measured experimentally for different waveguide positions and relative orientations (see Supplemental Material, IV [21]). We note that it is the collective effect of small distortions applied to every lattice site which gives rise to the topologically confined mode at the center of the vortex defect.

Experimental results.—Excitation of the vortex mode: First, we demonstrate a stationary photonic bulk zero mode. The vortex distortion is located at the center of the lattice, as shown in Figs. 2(a) and 2(b). In Fig. 2(c), comparing the experimental result (top) and the theoretical calculation (bottom), we see that they match very well. The waveguide mode intensity pattern is governed by Eqs. (4) and (5). The mode is excited using seven individual phase and amplitude tuned beams directed at waveguides on sublattice A carrying the majority of the mode [Fig. 2(d)]. We use a gradient descent algorithm to optimize the phases and amplitudes for maximum overlap with the zero mode (see Supplemental Material, II). The light in the zero mode is tightly confined to the center of the vortex and decays quickly outside the radius of the vortex $l_0 = 20$ μm, with a decay length governed by Eq. (4). Most of the intensity is confined to the sublattice which carries the bulk zero mode, as designed. Residual background originates from imperfect overlap of the exciting light field with the zero mode. Other imperfections arise from residual next-nearest neighbour coupling (see Supplemental Material, V). We estimate the ratio of nearest to next nearest neighbor coupling strength to be less than 5%. To quantify the degree to which this intensity pattern represents the zero mode, we introduce the ratio of light intensity between the two sublattices:

$$\gamma_{AB} = \frac{\text{light intensity in sublattice } A}{\text{light intensity in sublattice } B} \tag{6}$$

as a measure of fidelity for the excitation of the mode, which should be confined to one sublattice only. For a mode confined to sublattice A, we expect $\gamma_{AB} \gg 1$. The measured mode displayed in the top panel of Fig. 2(c) has $\gamma_{AB} = 4.8$. To ensure we only consider contributions from the zero mode, we integrate the light intensity within a 30 μm radius around the vortex center.

Adiabatic translation of the zero mode: Next, we translate the vortex zero mode transversely across the waveguide lattice by adiabatically shifting the vortex from one side of the lattice to the other by around 100 μm. In the experiment, a 9 cm long chip is used to ensure adiabatic translation of the zero mode. We can observe transverse translation of the zero-mode with most of the transmitted intensity confined around the center of the shifted vortex and in the correct sublattice [with a ratio of $\gamma_{AB} = 4.7$, Fig. 3(a), top panel]. The measured mode is no longer

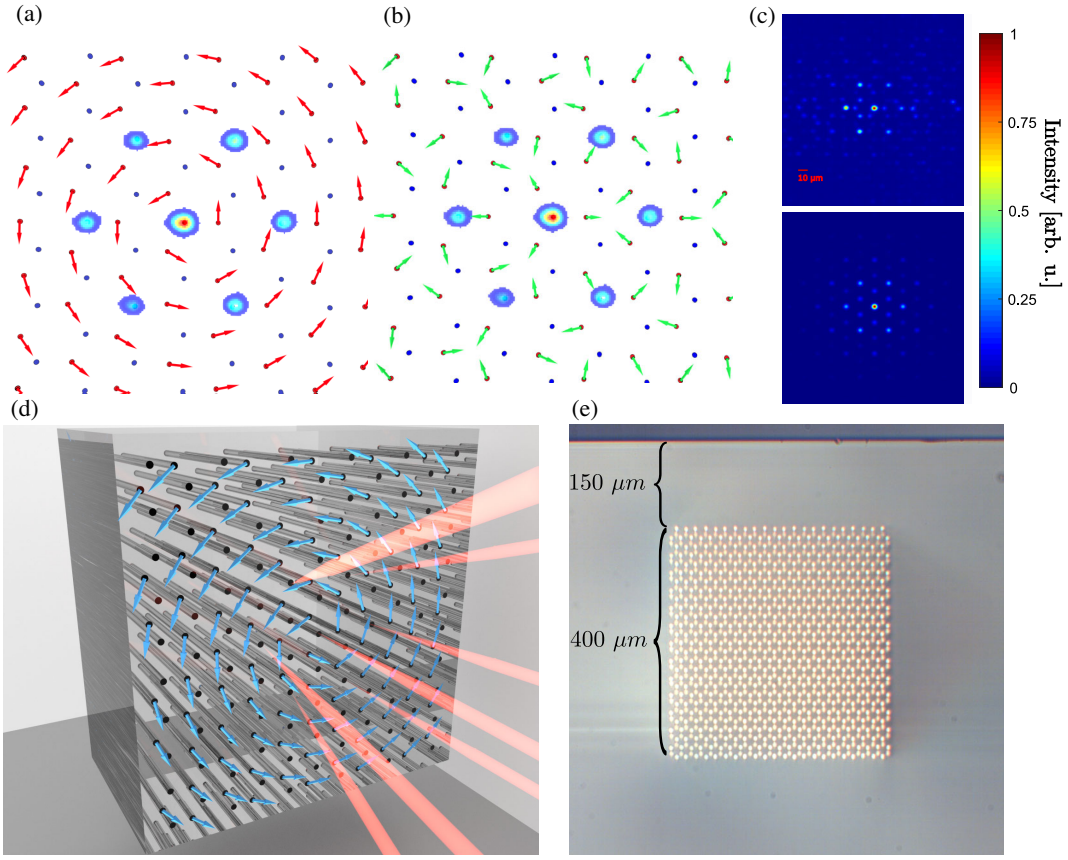

FIG. 2. (a) Photonic lattice with $\Delta(\mathbf{r})$ represented by red arrows. Bulk zero-mode intensity for dominant modes indicated at the center of the vortex. For visualizing the order parameter, the complex function $\Delta(\mathbf{r})$ is mapped onto a vector field through the correspondence $\mathbb{C} \rightarrow (\mathrm{Re}[\Delta(\mathbf{r})], \mathrm{Im}[\Delta(\mathbf{r})])$. (b) Shift of the waveguide positions from the graphene lattice configuration, which implements the topological vortex distortion, indicated by green arrows. (c) Comparison between the camera image of an observed stationary topological bulk zero mode (top) and the theoretical model (bottom). The theory has been convolved with a Gaussian to approximate the modes of the waveguides. (d) Illustration of multibeam excitation of the photonic lattice. An array of phase and amplitude tuned beams directed at individual waveguides carrying the majority of the intensity is used to achieve coherent excitation of the zero mode in the center of the vortex. (e) Image of the end facet of the silica chip, showing the full lattice of 1192 waveguides.

symmetrical, likely due to small variations in waveguide lattice fabrication which can easily shift the relative intensities within waveguides in the zero mode. In the bottom panel of Fig. 3(a), we show what happens if we try to excite the mode at a position in the lattice where there is no vortex present. As expected, we are not able to excite a mode and see no light transport. The ratio of intensities is $\gamma_{AB} = 0.67$.

Topological protection: To demonstrate that the zero mode is topologically protected against random errors of the lattice, we deliberately introduce an error to the position of the waveguides by shifting them by a random distance, sampled from a two-dimensional uniform distribution, where the radius r_d of the distribution corresponds to the maximum shift applied. We note that our mode is protected against any error which preserves chiral symmetry, such as random errors in waveguide position. In Fig. 4, we show the recoded zero modes at four different distortion levels with $r_d = 0$, 200, 400, 600 nm, respectively. The systematic topological distortion, which is introduced to the hexagonal lattice for the formation of the vortex, is approximately 850 nm. We can observe that the zero mode remains visible even when large random errors in waveguide position are introduced. The larger the error distortion, the more light leaks into the other sublattice. We measure a steadily decreasing amount of light in the correct sublattice $\gamma_{AB} = 3.8$, 2.9, 2.2, 2.1 as the error distortion increases.

Methods.—Waveguide lattice: Our photonic crystal lattices are fabricated in glass through femtosecond laser direct writing [30] (see also Supplemental Material, III). By employing advanced aberration correction techniques [31], we are able to write waveguide lattices of good homogeneity in depths of up to 1 mm. The dimension of the waveguide lattice is around 400×400 μm. Each waveguide lattice consists of 1192 waveguides that are arranged to form a hexagonal lattice. The distance between lattice sites is around 10 μm.

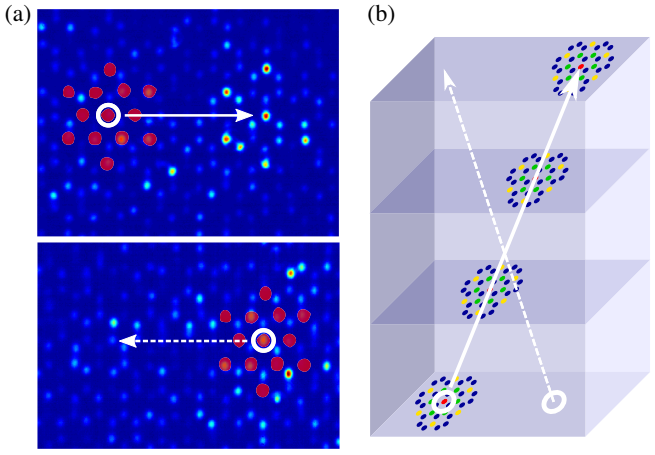

FIG. 3. (a) Top panel: Recorded bulk zero-mode transverse translation, in which the zero mode is translated from left [at input side schematically shown in (b)] to right (at the output side) of the lattice. Red dots indicate the positions of the 13 beams used to excite the zero mode at the input. The circled waveguide marks the position of the center at the input side. $\gamma_{AB} = 4.7$. Bottom panel: the same number of waveguides are excited on the input side of the lattice, where no vortex is present. At output side, $\gamma_{AB} = 0.67$. Also, the total light intensity in the displayed region is substantially less as most of the light is scattered into the rest of the lattice. The color scale is normalized to the brightest peak in both pictures. (b) Illustration of mode shifting by adiabatically translating (solid arrow) the center of the vortex (dotted pattern) along the longitudinal direction of the waveguide lattice; the dashed arrow indicates the direction the vortex moves in.

Mode excitation scheme: To excite the bulk zero mode, we developed a method based on an spatial light modulator to simultaneously illuminate multiple waveguides with beams of individually controlled phase and amplitude, as illustrated in Fig. 2(d). As coherent light source we use a laser diode at 785 nm. Multiple beams (up to 13 in the present work) are directed at individual waveguides near the center of the vortex. Phases and amplitudes of all beams are tuned to excite the zero mode (setup described in the Supplemental Material, I).

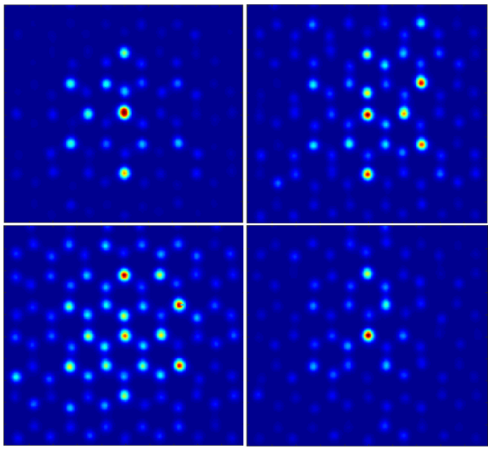

FIG. 4. Topological mode with random error distortions. Top left: no error, Top right: maximum 200 nm, Bottom left: maximum 400 nm, Bottom right: maximum 600 nm. The ratios of light intensity in the zero-mode sublattice to the nonmode supporting one are $\gamma_{AB} = 3.8$, 2.9, 2.2, 2.1, respectively. The color map of each image is normalized independently.

Conclusion.—We have demonstrated for the first time an experimental implementation of the Jackiw-Rossi model and observed the characteristic topological vortex zero mode in a photonic lattice. We excited the spatially delocalized mode at multiple sites, enabling us to resolve its structure. We showed that the mode can be adiabatically shifted across the photonic lattice and that it is topologically protected. Possible applications of these modes may lie in the protection of information encoded in quantum states against inevitable fabrication errors [11,32] in linear optical circuits by injecting multiple entangled particles into different protected vortex modes. Further, the degree of control we have demonstrated over these localized, protected topological bulk zero-modes may in the future enable applications probing the effects under exchange of multiple zero modes, as was suggested by Iadecola *et al.* [19]. These modes will accumulate a geometric phase when two of them are braided around each other.

We especially want to thank for their constructive input Claudio Chamon, Tom Iadecola, and Thomas Schuster. We thank Bryn Bell for sharing his knowledge in topological photonics. Furthermore, we would like to acknowledge Steve Simon and Glenn Wagner for providing valuable insights into solid state theory, Helen Chrzanowski for her experimental expertise, and Steve Kolthammer for initial discussions. We thank Patrick Salter for sharing his expertise in aberration correction techniques. A. J. M. is supported by the Buckee Scholarship at Merton College. J. G. work is supported by EPSRC grant (EP/M013243/1). This work was funded by the EPSRC through the Programme Grant No. EP/K034480/1, and by the European Union through the ERC Advanced Grant MOQUACINO. A. J. M. conducted the theoretical simulations, conceived the idea for the spatial light modulator based method of exciting multiple waveguides, and wrote the Letter with input from the other authors. J. G. built the adaptive femtosecond laser writing system, implemented the adaptive aberration correction, and fabricated the chips. A. J. M. and D. F. built and conducted the experiment. D. F. worked on the development and implementation of the method to control phase and amplitude of the light field. I. A. W., A. J. M., J. G., and M. J. B. conceived the project. I. A. W. and M. J. B. supervised the project.

Note added—Following our work, Noh *et al.* [33] have recently explored this type of defect, suggesting a geometric phase may be observed in a system consisting of a stationary, strongly localized defect mode and a simulated second defect. Moreover, our demonstration also provides

the possibility for further studying models employed in high energy physics, as well as new implementations of topological lasers other than those which have already been demonstrated in edge states [13,34]. Recently, X. Gao *et al.* [35] have implemented a Jackiw-Rossi–type defect in an optical microcavity using a silicon on oxide (SOI) platform. The authors envisage applications for vertical-cavity surface-emitting lasers (VCSELs) that use this mode for stable lasing. The topic of topological vortex defects has also recently been explored in other platforms: P. Gao *et al.* [36] realized a topological vortex defect in a sonic lattice. Chen *et al.* [37] have studied a mechanical analogue of the Jackiw-Rossi mode.

*adrian.menssen@physics.ox.ac.uk
†jun.guan@eng.ox.ac.uk

[1] M. Z. Hasan and C. L. Kane, Rev. Mod. Phys. **82**, 3045 (2010).
[2] J. C. Y. Teo and C. L. Kane, Phys. Rev. B **82**, 115120 (2010).
[3] X.-L. Qi and S.-C. Zhang, Rev. Mod. Phys. **83**, 1057 (2011).
[4] R. Jackiw and C. Rebbi, Phys. Rev. D **13**, 3398 (1976).
[5] R. Jackiw and P. Rossi, Nucl. Phys. **B190**, 681 (1981).
[6] E. Witten, Nucl. Phys. **B249**, 557 (1985).
[7] D. J. Thouless, M. Kohmoto, M. P. Nightingale, and M. den Nijs, Phys. Rev. Lett. **49**, 405 (1982).
[8] M. C. Rechtsman, Y. Plotnik, J. M. Zeuner, D. Song, Z. Chen, A. Szameit, and M. Segev, Phys. Rev. Lett. **111**, 103901 (2013).
[9] Y. Plotnik, M. C. Rechtsman, D. Song, M. Heinrich, J. M. Zeuner, S. Nolte, Y. Lumer, N. Malkova, J. Xu, A. Szameit *et al.*, Nat. Mater. **13**, 57 (2014).
[10] S. Stützer, Y. Plotnik, Y. Lumer, P. Titum, N. H. Lindner, M. Segev, M. C. Rechtsman, and A. Szameit, Nature (London) **560**, 461 (2018).
[11] J. Noh, W. A. Benalcazar, S. Huang, M. J. Collins, K. P. Chen, T. L. Hughes, and M. C. Rechtsman, Nat. Photonics **12**, 408 (2018).
[12] M. Hafezi, S. Mittal, J. Fan, A. Migdall, and J. M. Taylor, Nat. Photonics **7**, 1001 (2013).
[13] M. A. Bandres, S. Wittek, G. Harari, M. Parto, J. Ren, M. Segev, D. N. Christodoulides, and M. Khajavikhan, Science **359**, eaar4005 (2018).
[14] C. Chamon, C.-y. Hou, C. Mudry, and S. Ryu, Phys. Scr. **2012**, 014013 (2012).
[15] G. E. Volovik, J. Exp. Theor. Phys. Lett. **70**, 609 (1999).
[16] N. Read and D. Green, Phys. Rev. B **61**, 10267 (2000).
[17] C. Nayak, S. H. Simon, A. Stern, M. Freedman, and S. D. Sarma, Rev. Mod. Phys. **80**, 1083 (2008).
[18] C.-Y. Y. Hou, C. Chamon, and C. Mudry, Phys. Rev. Lett. **98**, 186809 (2007).
[19] T. Iadecola, T. Schuster, and C. Chamon, Phys. Rev. Lett. **117**, 073901 (2016).
[20] R. Jackiw and S. Y. Pi, Phys. Rev. Lett. **98**, 266402 (2007).
[21] See Supplemental Material at http://link.aps.org/supplemental/10.1103/PhysRevLett.125.117401 for a detailed description of our experimental methods, which includes Refs. [22–29].
[22] T.-L. Kelly and J. Munch, Appl. Opt. **37**, 5184 (1998).
[23] L. G. Neto, D. Roberge, and Y. Sheng, Appl. Opt. **35**, 4567 (1996).
[24] R. Dou and M. K. Giles, Appl. Opt. **35**, 3647 (1996).
[25] S. Chavali, P. M. Birch, R. Young, and C. Chatwin, Opt. Lasers Eng. **45**, 413 (2007).
[26] V. Bagnoud and J. D. Zuegel, Opt. Lett. **29**, 295 (2004).
[27] V. Arrizón, Opt. Lett. **28**, 1359 (2003).
[28] S. A. Goorden, J. Bertolotti, and A. P. Mosk, Opt. Express **22**, 17999 (2014).
[29] P. S. Salter, M. Baum, I. Alexeev, M. Schmidt, and M. J. Booth, Opt. Express **22**, 17644 (2014).
[30] A. Szameit and S. Nolte, J. Phys. B **43**, 163001 (2010).
[31] L. Huang, P. S. Salter, F. Payne, and M. J. Booth, Opt. Express **24**, 10565 (2016).
[32] M. C. Rechtsman, Y. Lumer, Y. Plotnik, A. Perez-Leija, A. Szameit, and M. Segev, Optica **3**, 925 (2016).
[33] J. Noh, T. Schuster, T. Iadecola, S. Huang, M. Wang, K. P. Chen, C. Chamon, and M. C. Rechtsman, arXiv:1907.03208.
[34] S. Mittal, E. A. Goldschmidt, and M. Hafezi, Nature (London) **561**, 501 (2018).10.1038/s41586-018-0478-3
[35] X. Gao, L. Yang, H. Lin, L. Zhang, J. Li, F. Bo, Z. Wang, and L. Lu, arXiv:1911.09540.
[36] P. Gao, D. Torrent, F. Cervera, P. San-Jose, J. Sánchez-Dehesa, and J. Christensen, Phys. Rev. Lett. **123**, 196601 (2019).
[37] C.-W. Chen, N. Lera, R. Chaunsali, D. Torrent, J. V. Alvarez, J. Yang, P. San-Jose, and J. Christensen, Adv. Mater. **31**, 1904386 (2019).